

# Efficiency of free auxiliary models in describing interacting fermions: from the Kohn-Sham model to the optimal entanglement model

Kristian Patrick,<sup>1</sup> Marcela Herrera,<sup>2</sup> Jake Southall,<sup>1</sup> Irene D’Amico,<sup>3,4</sup> and Jiannis K. Pachos<sup>1</sup>

<sup>1</sup>*School of Physics and Astronomy, University of Leeds, Leeds, LS2 9JT, United Kingdom*

<sup>2</sup>*Centro de Ciências Naturais e Humanas, Universidade Federal do ABC,  
Avenida dos Estados 5001, 09210-580 Santo André, São Paulo, Brazil*

<sup>3</sup>*Department of Physics, University of York, York, YO10 5DD, United Kingdom*

<sup>4</sup>*Instituto de Física de São Carlos, Universidade de São Paulo,  
CP 369, 13560-970, São Carlos, São Paulo, Brazil*

Density functional theory maps an interacting Hamiltonian onto the Kohn-Sham Hamiltonian, an explicitly free model with identical local fermion densities. Using the interaction distance, the minimum distance between the ground state of the interacting system and a generic free fermion state, we quantify the applicability and limitations of the Kohn-Sham model in capturing all properties of the interacting system. As a byproduct, this distance determines the optimal free state that reproduces the entanglement properties of the interacting system as faithfully as possible. When applied to the Fermi-Hubbard model we demonstrate that in the thermodynamic limit, rather surprisingly, the optimal free state provides an asymptotically exact representation of the ground state for all values of interaction coupling. The proposal of an optimal entanglement model, as the parent Hamiltonian of the optimal free state, opens up the exciting possibility of extending the systematic applicability of auxiliary free models into the non-perturbative, strongly-correlated regimes.

Undoubtably, interactions give rise to a wide range of quantum phases of matter with intriguing and exotic properties, ranging from many-body localisation [1] to the fractional quantum Hall effect [2]. Nevertheless, the theoretical investigation of interacting systems is often formidable due to their complexity [3–5]. A possible approach in studying interacting systems is to approximate them by free models that offer a simpler and intuitive description. To this aim, physicists, chemists and material scientists alike often use Density Functional Theory (DFT) [6–9]. In its basic formulation, DFT uniquely maps a many-body system to an auxiliary non-interacting one, known as the Kohn-Sham (KS) model [10], which has the same ground state fermion density as the interacting system. While it is known to fail in the strong correlation limit, the KS model has been used to estimate many-body properties other than the fermion density, such as band-structure calculations [9, 11], quantum work [12], and entanglement [13]. However, it is not known how optimal the KS model is within the set of all possible free fermion theories.

To quantify the applicability of the KS model we employ the concept of interaction distance,  $D_{\mathcal{F}}$  [14]. This distance measures how far the ground state of a given system is from the manifold of all free fermion states in terms of their quantum correlations [14–16]. The interaction distance also identifies the optimal free state, a state with entanglement properties as close as possible to the interacting system. We demonstrate that, in the perturbative (weak-interaction) regime, if  $D_{\mathcal{F}} \approx 0$  then the KS ground state is close to the optimal free state, with an error in determining *any* observable of the interacting system bounded by  $D_{\mathcal{F}}$ . We also show that, away from the perturbative regime the reliability of the KS model as an approximation can fail even if  $D_{\mathcal{F}} \approx 0$ . Indeed, interactions may “freeze” some fermionic degrees

of freedom used to build the KS model. To describe the interacting model as faithfully as possible in all coupling regimes we introduce the “optimal entanglement model”, with a Hamiltonian that has the optimal free state as its ground state. This alternative to the KS model reproduces all the properties of the interacting system, even in the strong-correlation regime, with an error bounded by  $D_{\mathcal{F}}$ .

To exemplify this approach we employ the Fermi-Hubbard model. By determining its interaction distance we quantify the regimes where the KS and the optimal entanglement models are good approximations to the interacting system and where they fail. Moreover, we numerically demonstrate that at half-filling, and by appropriately approaching the thermodynamic limit, the interaction distance tends to zero for any values of the interaction coupling. Hence, the optimal entanglement model can faithfully reproduce all properties of the Fermi-Hubbard model for all coupling regimes.

**Kohn-Sham and Optimal Entanglement Models.** Let us consider a Hamiltonian  $\hat{H} = \hat{K} + \hat{V} + \hat{W}$  on a lattice, built from a kinetic energy operator  $\hat{K}$ , a local potential operator  $\hat{V} = \sum_j^L v_j \hat{n}_j$ , where  $\hat{n}_j$  is the site-occupation operator, and a particle-particle interaction operator  $\hat{W}$ . At the core of lattice-DFT are the one-to-one correspondences between the ground state wave function  $|\psi\rangle$ , the corresponding ground state density  $\langle \hat{n}_j \rangle$  for  $j = 1, \dots, L$ , and the local potential [17] of an  $L$ -site many-body system [11]. With the ansatz of  $n$  and  $v$ -representability, these correspondences imply that there exists a unique non-interacting model, the so called Kohn-Sham model [10], which is subject to the same kinetic operator and having the same ground-state density as the original  $N$ -particle interacting system. Through this model, the density, and then in principle all other physical many-body properties [9], can be obtained. The



interacting system, while a non-zero  $D_{\mathcal{F}}$  bounds the errors in determining the entanglement properties of the interacting model. Away from the perturbative regime it is possible that bound (4) fails, by having  $\rho^{\text{KS}}$  far from  $\rho^{\text{int}}$  even if  $D_{\mathcal{F}} \approx 0$ , as shown in Fig. 1. Nevertheless,  $\rho^{\text{opt}}$  would still provide a faithful description of  $\rho^{\text{int}}$ .

The parent Hamiltonian of the optimal free state can be used to define a suitable auxiliary free model that identifies the effective degrees of freedom of the interacting model for all coupling regimes. When  $D_{\mathcal{F}} \approx 0$  such an auxiliary model not only faithfully reproduces the entanglement properties of the interacting model but, due to Eq. (2), it can also estimate all of its observables, such as the local fermion densities. This ‘optimal entanglement’ model generalises the KS model that can fail to reproduce the entanglement properties even if  $D_{\mathcal{F}} \approx 0$ . In fact, strong interactions may not only change the effective local fermion potential,  $\hat{V}$ , but also the kinetic term,  $\hat{K}$ . To build this auxiliary model one first needs to identify the effective fermionic degrees of freedom that correspond to the quantum correlations of the model. If  $D_{\mathcal{F}} \approx 0$  for strong interactions then the number of fermionic degrees of freedom of the emerging free theory can be either the same or smaller than the initial theory without the interaction term: interactions could freeze some of the initial fermionic degrees of freedom but they cannot increase their number. To exemplify this procedure we apply it next to the Fermi-Hubbard model at half-filling.

**The Fermi-Hubbard Model.** The 1D Hubbard model [20] has successfully reproduced a number of physical phenomena, including interaction-driven quantum phase transitions [21]. In some limits it has exact solutions [22, 23] and has been studied via many numerical techniques including DFT [11]. It comprises spin- $\frac{1}{2}$  fermions with a creation (annihilation) operator  $c_{j,\sigma}^\dagger$  ( $c_{j,\sigma}$ ) at site  $j$  and spin  $\sigma \in \{\uparrow, \downarrow\}$ , with Hamiltonian

$$\hat{H} = \sum_{j,\sigma} \left[ -J \left( c_{j,\sigma}^\dagger c_{j+1,\sigma} + \text{h.c.} \right) + \nu_j \hat{n}_{j,\sigma} \right] + U \sum_j \hat{n}_{j,\uparrow} \hat{n}_{j,\downarrow} \quad (5)$$

where  $\hat{n}_{j,\sigma} = c_{j,\sigma}^\dagger c_{j,\sigma}$  is the number operator,  $J$  is the tunnelling strength,  $U$  is the on-site particle-particle interaction strength, and  $\nu_j$  is the site-dependent potential. For repulsive interactions,  $U > 0$ , the model in the thermodynamic limit has two phases: for small  $U$  (perturbative regime) it is described by the Luttinger liquid phase, where local fermion densities are free to change, and the large  $U$  limit is described by the Mott-insulator phase, where local densities are frozen by Coulomb repulsion [21]. Hence, it is an ideal system to demonstrate the applicability of the optimal entanglement model.

For the discussion to remain general, we probe the behaviour of the Hubbard model in the thermodynamic limit and perform a size scaling analysis of the interaction distance [24]. The ansatz used is  $D_{\mathcal{F}} \approx L^{-\zeta} f((U - U_c) L^{1/\nu})$ , where  $L$  is the system size,  $U_c$  a critical value of  $U$ ,  $f$  is a smooth function, and  $\zeta, \nu$  are

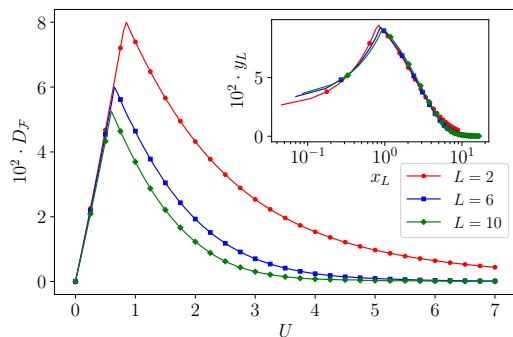


FIG. 2. The interaction distance  $D_{\mathcal{F}}$  for the Hubbard model with  $J = 1$ , all local potentials  $\nu_j$  being zero except  $\nu_1 = 0.5$  and chains of length  $L = 2$  (red), 6 (blue), and 10 (green). (Inset) Finite size scaling analysis of  $D_{\mathcal{F}}$  with collapsed variables  $x_L = (U - U_c)L^{1/\nu}$  and  $y_L = D_{\mathcal{F}}L^\zeta$ . The optimal critical exponents  $\nu \approx 2.573$ ,  $\zeta \approx 0.243$ , and  $U_c \approx 0.215$ . The scaling collapse shows that  $D_{\mathcal{F}} \rightarrow 0$  as  $L \rightarrow \infty$  for all  $U$ . Therefore, in the limit  $L \rightarrow \infty$  the Hubbard model can be accurately described by free fermions.

the critical exponents [14]. We consider system sizes of the form  $L = 4k + 2$ ,  $k = 0, 1, 2, \dots$  at half filling, where the system has a unique ground state with a symmetric Fermi sea [25]. In Fig. 2 we show both the unscaled value of the interaction distance and the scaling collapse for chains of length  $L = 2, 6$ , and 10. The obtained critical exponents are  $\nu \approx 2.573$ ,  $\zeta \approx 0.243$ , and  $U_c \approx 0.215$ . Even for these relatively small system sizes the correlation length exponent is consistent with the known CFT result  $\nu = 2.5$  [26]. As  $\zeta > 0$  the interaction distance decreases with system size, taking the value zero in the thermodynamic limit for all values of  $U$ . Hence, the interacting model has ground state correlations, and thus a low energy description [27], that can be faithfully represented by free fermions for any value of  $U$ . This generalises the known result that the Fermi-Hubbard model is free for large couplings  $U$  [21].

It is possible to construct an auxiliary free model with ground state correlations that converge polynomially fast, with system size, to the correlations of the interacting model in the insulating phase [28, 29]. The  $L \rightarrow \infty$  parent Hamiltonian may be constructed from non-interacting spinless fermions with both nearest neighbour and next-nearest neighbour hopping terms [28, 29]:

$$\hat{H}_{\text{aux}}^{\text{TD}} = -J \sum_{j=1}^{L-1} \left( c_j^\dagger c_{j+1} + c_{j+1}^\dagger c_j \right) - \frac{J'}{2U} \sum_{j=1}^{L-2} \left( c_j^\dagger c_{j+2} + c_{j+2}^\dagger c_j \right). \quad (6)$$

The coupling  $J'$  could be used as a fitting parameter to optimise the behaviour of  $\hat{H}_{\text{aux}}^{\text{TD}}$ . For simplicity we take here  $J' = 1$ . In Fig. 3,  $D_{\text{tr}}(\rho^{\text{int}}, \rho^{\text{aux}})$  is calculated, where  $\rho^{\text{aux}}$  is the ground state reduced density matrix

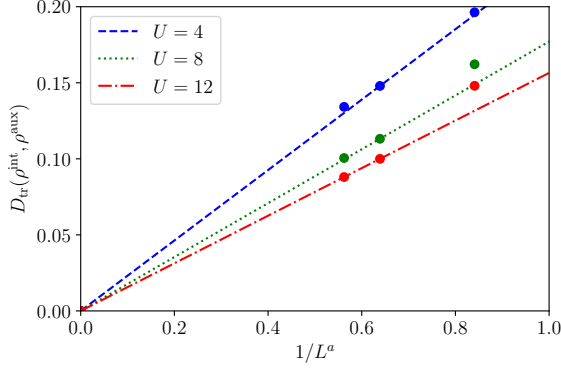


FIG. 3. The trace distance  $D_{\text{tr}}(\rho^{\text{int}}, \rho^{\text{aux}})$ , where  $\rho^{\text{aux}}$  is the ground state of  $\hat{H}_{\text{aux}}^{\text{TD}}$ , at half-filling with varying  $L = 2, 6, 10$ ,  $J = 1$ ,  $J' = 1$  and  $U = 4$  (blue),  $U = 8$  (green),  $U = 12$  (red). The lines are fixed at  $1/L^a = 0$  and fitted to the  $L = 6$  and  $10$  points. We observe that even for these relatively small system sizes  $D_{\text{tr}}(\rho^{\text{int}}, \rho^{\text{aux}}) \rightarrow 0$  as  $L \rightarrow \infty$ , due to the positive scaling exponent  $a = 0.25$ . The  $L = 2$  point (far right) shows deviation due to its small size.

of  $\hat{H}_{\text{aux}}^{\text{TD}}$  at half-filling. For each value of  $U$  the distance scales polynomially with system size due to finite size effects. However, it is clear that in the limit  $L \rightarrow \infty$ ,  $D_{\text{tr}}(\rho^{\text{int}}, \rho^{\text{aux}}) \rightarrow 0$  for any choice of  $U$ . Hence, even if  $\hat{H}_{\text{aux}}^{\text{TD}}$  is not optimally constructed, its ground state,  $\rho^{\text{aux}}$ , efficiently describes the entanglement properties of the interacting system in the thermodynamic limit.

To study in detail the efficiency of the KS and the optimal entanglement models in representing the interacting ground state, we focus on the half-filled Hubbard dimer ( $L = 2$ ). At this size interactions are expected to have a dominant effect as the dimer corresponds to the situation farthest away from the thermodynamic limit, where  $D_{\mathcal{F}} \rightarrow 0$ . For this system size the KS model can be numerically determined exactly. There also exists exact solutions for the optimal free state of a four level system, see Appendices, that can be employed here. Moreover, we can analytically determine the optimal entanglement model, that reproduces exactly the entanglement spectrum of the optimal free state in the insulating phase. Focused on this regime where the KS model is known to fail, we have that the optimal auxiliary Hamiltonian is given by

$$\hat{H}_{\text{aux}} = -J \left( c_1^\dagger c_3 + c_3^\dagger c_1 \right) - J \left( c_2^\dagger c_4 + c_4^\dagger c_2 \right) - \frac{\mu}{2} c_1^\dagger c_1. \quad (7)$$

The chemical potential,  $\mu$ , can be obtained explicitly, giving the simple form  $\mu \approx JU$  when  $U$  is large (see Appendices).

The behaviour of the corresponding ground state reduced density matrices  $\rho^{\text{int}}$ ,  $\rho^{\text{KS}}$ ,  $\rho^{\text{opt}}$ , and  $\rho^{\text{aux}}$ , are given in Fig. 4. Note that  $D_{\mathcal{F}} \approx 0$  for all values of  $U$  away from the critical region. Surprisingly, the KS ground state closely approximates the optimal free state

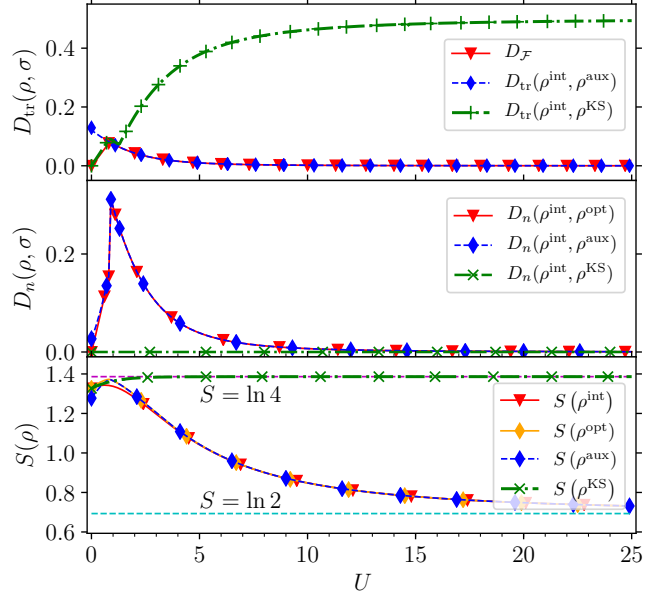


FIG. 4. (Top) Trace distance, (Middle) natural metric, and (Bottom) entanglement entropy for the interacting,  $\rho^{\text{int}}$ , optimal,  $\rho^{\text{opt}}$ , KS,  $\rho^{\text{KS}}$ , and auxiliary,  $\rho^{\text{aux}}$ , reduced density matrices, as a function of the interaction coupling  $U$ , for  $L = 2$ ,  $J = 1$ , total spin  $S_z = 0$ , and  $\nu_1 - \nu_2 = 0.5$ . In the perturbative limit the KS is a good approximation to the optimal entanglement model which describes spin-1/2 free fermions. In the large  $U$  limit the KS model fails, while both the optimal and auxiliary states that describe spinless free fermions, provide faithful representations of the local densities (Middle) and the entanglement entropy (Bottom) of the interacting system. For large  $U$  the entanglement entropy of the KS model tends to  $S = \ln 4$  corresponding to the maximally entangled state  $|\psi\rangle = (|\uparrow\downarrow, 0\rangle + |\uparrow, \downarrow\rangle + |\downarrow, \uparrow\rangle + |0, \uparrow\downarrow\rangle)/2$  while the interacting, optimal and auxiliary systems tend to  $S \approx \ln 2$  that correspond to  $|\psi\rangle = (|\uparrow, \downarrow\rangle + |\downarrow, \uparrow\rangle)/\sqrt{2}$ , signalling the freezing of double occupations due to interactions.

not only in the perturbative, but also in the intermediate coupling regime,  $U \sim |J|, |\nu_j|$ , up to the phase transition region. Here the trace distance between all pairs of states is small, so the KS is both exact in fermion density and also reproduces the ground state correlations of the optimal model accurately. In the strong coupling regime,  $U \gg |J|, |\nu_j|$ , the KS model fails to reproduce the correlation properties of the interacting model, as it still describes correlations between spinful free fermions. This is in contrast to the optimal free model that, in that regime, is described by spinless free fermions. These degrees of freedom faithfully capture the quantum correlations of the interacting model, as shown in Fig. 4 (Bottom). Nevertheless, they only approximate its local densities, as shown in Fig. 4 (Middle), with an error that is bounded by the value of  $D_{\mathcal{F}}$ , as dictated by Eq. (3). The local densities identify the change of the degrees of freedom from one optimal model to the other via the observed kink.

From the properties of the optimal free state we see that the effect of the strong interactions is to freeze the local fermion populations to  $n_j = 1$  as an eigenvalue of the local density operator. This can be witnessed by the behaviour of the entanglement entropy,  $S$ . In Fig. 4 we observe that the KS model saturates to the value  $S = \ln 4$  due to both spin and population fluctuations. In contrast, the interacting model has entanglement entropy that tends to  $S = \ln 2$  as  $U \rightarrow \infty$ , due to only spin correlations. As the interaction distance is approaching zero for large  $U$ , then the optimal free model with Hamiltonian (7) faithfully reproduces both the local densities as well as the correlation properties of the interacting system, as shown in Fig. 4. Hence, unlike the KS model, it provides a faithful representation of the interacting theory.

To schematically present why the optimal free model succeeds in faithfully representing the interacting system for large  $U$ , while the KS model fails, we refer to the schematic in Fig. 1. From the above analysis of the dimer model we observe that interactions have the effect of moving the optimal free state from describing free spinful fermions (manifold  $\mathcal{F}$ ) towards the description of free spinless fermions (manifold  $\mathcal{F}'$ ). Due to the fixed form of the kinetic term of the KS Hamiltonian, its corresponding reduced density matrix will always live in  $\mathcal{F}$ . By choosing the auxiliary model to optimise over entanglement, its degrees of freedom can change from  $\mathcal{F}$  to  $\mathcal{F}'$  that better describes the interacting system at large couplings  $U$ . Thus, the optimal free model is able to reproduce all the properties of the interacting system for all  $U$ , with an error that is bounded by  $D_{\mathcal{F}}$ .

**Conclusions.** With the help of the interaction distance,  $D_{\mathcal{F}}$ , we are able to identify the free model that

approximates the interacting system by optimising over the corresponding entanglement properties. We demonstrate that when the interaction distance is small then the optimal entanglement model reproduces all observables of the interacting system with accuracy bounded by  $D_{\mathcal{F}}$ . As such, it provides an accurate modelling of the low energy behaviour of the system [14, 27]. The KS model, on the other hand, finds local densities exactly for all strengths of interactions, but can dramatically fail to obtain entanglement features even when the interaction distance is small. Motivated by these results we envisage that a method inspired by DFT, where the optimisation of the free model is performed with respect to entanglement properties rather than local densities, can faithfully approximate strongly interacting systems.

To exemplify the diagnostic power of the interaction distance, we considered the Fermi-Hubbard model. We numerically demonstrated the surprising result that this model at half-filling can be represented exactly in the thermodynamic limit ( $L = 4k + 2 \rightarrow \infty$ ) by free fermions for any value of its interaction coupling  $U$ . This generalises the well known result that the Hubbard model is free in the large  $U$  limit for any system size [21].

**Acknowledgements.** We would like to thank Pasquale Calabrese, Konstantinos Meichanetzidis, Zlatko Papić, and Christopher J. Turner for inspiring conversations. Fig. 1 was designed by Jack White. KP, JS, and JKP acknowledge support by the EPSRC grant EP/I038683/1. MH acknowledges support from FAPESP (grant no.2014/02778-1) IDA and MH acknowledge support from the Royal Society through the Newton Advanced Fellowship scheme (Grant no. NA140436) and IDA from CNPq (Grant: PVE-Processo: 401414/2014-0).

- 
- [1] R. Nandkishore and D. A. Huse, *Con. Mat. Phys.* **6**, 15 (2015).
  - [2] R. B. Laughlin, *Phys. Rev. Lett.* **50**, 1395 (1983).
  - [3] F. Verstraete, V. Murg, and J. Cirac, *Physics* **57**(2), 143 (2008).
  - [4] G. Vidal, *Phys. Rev. Lett.* **101**, 110501 (2008).
  - [5] M. P. Nightingale and C. J. Umrigar, *Springer Science & Business Media* **525**, (1998).
  - [6] P. Hohenberg and W. Kohn, *Phys. Rev. B* **136**, B846-B871 (1964).
  - [7] R. O. Jones and O. Gunnarsson, *Rev. Mod. Phys.* **61**, 689 (1989).
  - [8] R. O. Jones, *Rev. Mod. Phys.* **87**, 897 (2015).
  - [9] K. Capelle, *Braz. J. Phys.* **36**, 1318 (2006).
  - [10] W. Kohn and L. Sham, *Phys. Rev.* **140**, A1133 (1965).
  - [11] K. Capelle and V. L. Campo, *Phys. Rep.* **528**, 91 (2013).
  - [12] M. Herrera, R. Serra, and I. D'Amico, *Sci. Rep.* **7**, 4655 (2017).
  - [13] J. P. Coe, A. Sudbery, I. D'Amico, *Phys. Rev. B* **77**, 205122 (2008).
  - [14] C. Turner, K. Meichanetzidis, Z. Papić, and J. Pachos, *Nat. Comm.* **8**, 14926 (2017).
  - [15] K. Meichanetzidis, C. Turner, A. Farjami, Z. Papić, and J. Pachos, *Phys. Rev. B* **97**, 125104 (2018).
  - [16] J. K. Pachos and Z. Papić, *arXiv:1803.06812*.
  - [17] J. P. Coe, I. D'Amico and V. V. Franca, *EPL* **110**, 63001 (2015).
  - [18] M. A. Nielsen and I. Chuang, *Quantum computation and quantum information*, (2002).
  - [19] I. D'Amico, J. Coe, V. V. Franca, and K. Capelle, *Phys. Rev. Lett.* **106**, 050401 (2011).
  - [20] J. Hubbard, *Proc. R. Soc. London, Sec. A* **276**, 238 (1963).
  - [21] F. H. Essler, H. Frahm, F. Göhmann, A. Klümper, and V. E. Korepin, *The one-dimensional Hubbard model*, Cambridge University Press, (2005).
  - [22] E. Lieb and F. Wu, *Phys. Rev. Lett.* **20**, 1445 (1968).
  - [23] J. Carmelo and D. Baeriswyl, *Phys. Rev. B* **37**, 13 (1988).
  - [24] The optimisation code for finding the interaction distance can be found at <https://theory.leeds.ac.uk/interaction-distance/code/>.
  - [25] F. H. L. Essler, A. M. Läuchli and P. Calabrese, *Phys. Rev. Lett.* **110**, 115701 (2013).
  - [26] N. Kawakami and S.-K. Yang, *J. Phys.: Condens. Matter*

- 3**, 5983 (1991).  
 [27] H. Li and F. Haldane, Phys. Rev. Lett. **101**, 010504 (2008).  
 [28] M. Ogata and H. Shiba, Phys. Rev. B **41**, 2326 (1990).  
 [29] M. Ogata, T. Sugiyama, and H. Shiba, Phys. Rev. B **43**, 8401 (1991).

### Appendix A: Bounding observables with $D_{\mathcal{F}}$

Consider the expectation value of an observable  $\mathcal{O}$  for two density matrices  $\rho$  and  $\sigma$  given by  $\langle \mathcal{O} \rangle_{\rho} = \text{tr}[\mathcal{O}\rho]$  and  $\langle \mathcal{O} \rangle_{\sigma} = \text{tr}[\mathcal{O}\sigma]$ , respectively. To compare these expectation values we define their difference by the metric

$$d_{\mathcal{O}}(\rho, \sigma) = \left| \langle \mathcal{O} \rangle_{\rho} - \langle \mathcal{O} \rangle_{\sigma} \right|, \quad (\text{A1})$$

which reduces to  $d_{\mathcal{O}} = |\text{tr}[\mathcal{O}(\rho - \sigma)]|$ . Let us express  $\rho - \sigma$  in its diagonal basis,  $(\rho - \sigma) = \sum_k \phi_k |\phi_k\rangle\langle\phi_k|$ , where  $\phi_k$  are the eigenvalues of  $\rho - \sigma$ . Then, via direct substitution into  $d_{\mathcal{O}}$ , we find that

$$d_{\mathcal{O}} = \left| \text{tr} \left[ \mathcal{O} \sum_k \phi_k |\phi_k\rangle\langle\phi_k| \right] \right| \quad (\text{A2})$$

$$= \left| \sum_k \langle \phi_k | \mathcal{O} | \phi_k \rangle \phi_k \right| \quad (\text{A3})$$

$$\leq \left| \max_k \langle \phi_k | \mathcal{O} | \phi_k \rangle \sum_k \phi_k \right| = C_{\mathcal{O}} \left| \sum_k \phi_k \right|, \quad (\text{A4})$$

where  $C_{\mathcal{O}} = \left| \max_k \langle \phi_k | \mathcal{O} | \phi_k \rangle \right| \geq 0$ . It then follows that

$$d_{\mathcal{O}} \leq C_{\mathcal{O}} \sum_k |\phi_k| = C_{\mathcal{O}} \text{tr} |\rho - \sigma|, \quad (\text{A5})$$

where the final equality explicitly contains the definition of the interaction distance when  $\sigma = \rho^{\text{opt}}$ . Therefore, when  $\rho = \rho^{\text{int}}$  and  $\sigma = \rho^{\text{opt}}$  the difference in expectation values are bounded by the interaction distance, i.e.

$$\left| \langle \mathcal{O} \rangle_{\rho^{\text{int}}} - \langle \mathcal{O} \rangle_{\rho^{\text{opt}}} \right| \leq C_{\mathcal{O}} D_{\mathcal{F}}, \quad (\text{A6})$$

with  $C_{\mathcal{O}} = \frac{1}{2} \max_k \langle \phi_k | \mathcal{O} | \phi_k \rangle$  that depends only on the operator  $\mathcal{O}$ .

### Appendix B: Bounding $D_n(\rho^{\text{KS}}, \rho^{\text{opt}})$ by $D_{\mathcal{F}}$

The result in Eq. (A6) can be applied directly to the definition of the natural metric given in the main text. Let  $\mathcal{O} = \hat{n}_j$  that is the local fermion density at site  $j$  within the subspace of the reduced density matrix. To arrive at the definition of the natural metric we must sum over all sites. Then, Eq. (A6) becomes

$$\sum_j \left| \langle \hat{n}_j \rangle_{\rho^{\text{int}}} - \langle \hat{n}_j \rangle_{\rho^{\text{opt}}} \right| \leq \sum_j C_j D_{\mathcal{F}}. \quad (\text{B1})$$

The left hand side of this equality is the definition of the natural metric and the right hand side consists of a constant  $C = \sum_j C_j$  multiplied by the interaction distance. The bound reduces to

$$D_n(\rho^{\text{int}}, \rho^{\text{opt}}) \leq C D_{\mathcal{F}}. \quad (\text{B2})$$

Due to the key property of the Kohn-Sham model, that  $\langle \hat{n}_j \rangle_{\rho^{\text{int}}} = \langle \hat{n}_j \rangle_{\rho^{\text{KS}}}$ , the bound may be cast in terms of the optimal and Kohn-Sham ground states

$$D_n(\rho^{\text{KS}}, \rho^{\text{opt}}) \leq C D_{\mathcal{F}}. \quad (\text{B3})$$

Therefore, when  $D_{\mathcal{F}} \approx 0$  the optimal free state shares the same local fermion densities as the interacting and Kohn-Sham ground states.

### Appendix C: Trace distance bounding in perturbative limit

Here we prove that within the perturbative limit, i.e. when  $n_F = n + \delta n$ , with  $n_F$  the ground state density of the optimal free state,  $n$  the ground state density of the interacting/KS model, and  $\delta n$  a small linear response, then  $D_{\text{tr}}(\rho^{\text{KS}}, \rho^{\text{opt}}) \leq c D_{\mathcal{F}}$ , with  $c > 0$ . First consider the limit  $\delta n \rightarrow 0$ . In this limit  $D_{\text{tr}}(\rho^{\text{KS}}, \rho^{\text{opt}}) \rightarrow 0$  and  $D_{\mathcal{F}} \rightarrow 0$ , so that the inequality above is satisfied by the equality  $0 = c \cdot 0$ . Next, consider the linear response to be small and non-zero. We have already shown that the density metric is bound by the interaction distance. When DFT Hohenberg-Kohn-type theorems apply, any property of a pure state interacting system described by a Hamiltonian  $\hat{H} = \hat{K} + \hat{W} + \hat{V}$ , can be written as a functional of the system ground state density. So, in particular, the (non-diagonal) density matrix elements can also be written as a functional of the ground state density, leading to

$$D_{\text{tr}}(\rho^{\text{KS}}, \rho^{\text{opt}}) = D_{\text{tr}}[n_F, n] = D_{\text{tr}}[\delta n, n]. \quad (\text{C1})$$

For small  $\delta n$ , we can approximate  $D_{\text{tr}}(\rho^{\text{opt}}, \rho^{\text{KS}})$  around  $\delta n$ :

$$D_{\text{tr}}(\rho^{\text{KS}}, \rho^{\text{opt}})[\delta n, n] = D_{\text{tr}}[0, n] + \frac{\delta D_{\text{tr}}}{\delta n} \Big|_{\delta n=0} \delta n + \frac{\delta^2 D_{\text{tr}}}{\delta n^2} \Big|_{\delta n=0} (\delta n)^2 + \dots, \quad (\text{C2})$$

so that

$$D_{\text{tr}}(\rho^{\text{KS}}, \rho^{\text{opt}})[\delta n, n] \approx \frac{\delta^2 D_{\text{tr}}}{\delta n^2} \Big|_{\delta n=0} (\delta n)^2 > 0, \quad (\text{C3})$$

where expressions (C3) hold due to  $\delta n = 0$  being a minimum (and the trace distance being a metric). Similarly, we can approximate the density metric about the minimum:

$$D_n(\rho^{\text{KS}}, \rho^{\text{opt}}) = D_n(\rho^{\text{KS}}, \rho^{\text{opt}})[\delta n, n] \quad (\text{C4})$$

$$\approx \frac{\delta^2 D_n}{\delta n^2} \Big|_{\delta n=0} (\delta n)^2 > 0 \quad (\text{C5})$$



Using Eq.'s (C3) and (C5), and up to higher orders than  $(\delta n)^2$  in  $\delta n$ , we can then write

$$D_{\text{tr}}(\rho^{\text{KS}}, \rho^{\text{opt}})[\delta n, n] \approx f(n) \cdot D_n(\rho^{\text{KS}}, \rho^{\text{opt}}), \quad (\text{C6})$$

where  $f(n) = \frac{\delta^2 D_{\text{tr}}}{\delta n^2} \Big|_{\delta n=0} \left( \frac{\delta^2 D_n}{\delta n^2} \Big|_{\delta n=0} \right)^{-1}$  is a functional of  $n$ , but for a given  $n$  it will be a number greater than zero. Using Eq. (B3) we then obtain

$$D_{\text{tr}}(\rho^{\text{KS}}, \rho^{\text{opt}}) \leq f(n) \cdot C D_{\mathcal{F}}. \quad (\text{C7})$$

#### Appendix D: An optimal entanglement model for the Hubbard Dimer at half-filling

In order to exemplify the construction of a free auxiliary model that is accurate (within the error of  $D_{\mathcal{F}}$ ) in not only local fermion density but also all other properties, we restrict ourselves to the Hubbard dimer at half filling. The Hilbert space is spanned by the basis  $\{|\uparrow\downarrow, 0\rangle, |\uparrow, \downarrow\rangle, |\downarrow, \uparrow\rangle, |0, \uparrow\downarrow\rangle\}$ , where the basis state  $|x, y\rangle = |x\rangle \otimes |y\rangle$  corresponds to  $x$  fermions at the first site and  $y$  fermions at the second. In this basis the Hamiltonian, Eq. (5) of the main text, in matrix form is

$$\hat{H} = \begin{pmatrix} U + 2\nu_1 & -J & J & 0 \\ -J & \nu_1 + \nu_2 & 0 & -J \\ J & 0 & \nu_1 + \nu_2 & J \\ 0 & -J & J & U + 2\nu_2 \end{pmatrix}. \quad (\text{D1})$$

Eigenstates of this Hamiltonian have both occupation and spin degrees of freedom that can be varied by tuning the tunnelling and repulsive interaction strength. By observation of the optimal free state entanglement spectrum in the insulating phase, found using the exact solutions quoted previously, it can be seen that there exists a double degeneracy. In order to reproduce this optimal free entanglement spectrum, we construct an auxiliary model with two spinless non-interacting fermions hopping on separate two site chains. By allowing the fermions to hop freely it is possible to obtain an entanglement entropy of  $S = \ln 4$ . Then, by appropriately tuning a chemical potential on a single site as interactions increase, it is possible to match exactly the double degeneracy of the optimal free entanglement spectrum, as the entropy reduces to  $S = \ln 2$  (see Fig. 4 (Bottom) of the main text). Such a spectrum can be reproduced by the following Hamiltonian:

$$\hat{H}_{\text{aux}} = -J(c_1^\dagger c_3 + c_3^\dagger c_1) - J(c_2^\dagger c_4 + c_4^\dagger c_2) - \frac{\mu}{2} c_1^\dagger c_1 \quad (\text{D2})$$

where  $\mu = 2 \left[ \sqrt{\frac{\rho_1^{\text{opt}}}{\rho_2^{\text{opt}}}} - \sqrt{\frac{\rho_2^{\text{opt}}}{\rho_1^{\text{opt}}}} \right]$  and  $(\rho_1^{\text{opt}}, \rho_2^{\text{opt}})$  are the two distinct optimal entanglement levels. The partition that returns the desired spectrum separates sites 1, 2 into subsystem  $A$  and sites 3, 4 into subsystem  $B$ .

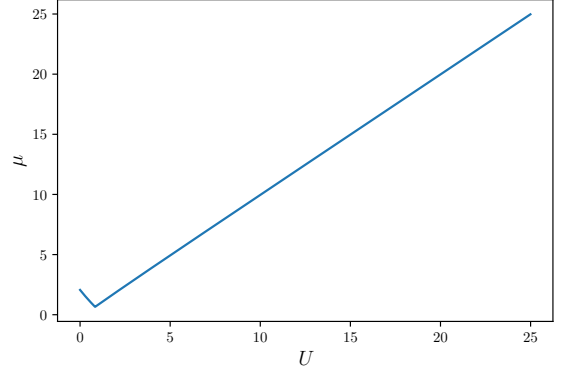


FIG. 5. Behaviour of the chemical potential  $\mu$ , for the  $L = 2$  optimal entanglement mode at half-filling, against interaction strength of the interacting model,  $U$ . In the strong interaction regime we find  $\mu \approx JU$  to a very good approximation.

It can be easily seen that  $\mu = \mu(J, \nu_j, U)$  as the optimal free entanglement levels are functions of the couplings of the interacting model. Further, as seen in Fig. 5, we observe a linear behaviour  $\mu \approx JU$  within the insulating phase.

#### Appendix E: Exact optimal free state for a four level system

By careful consideration of the interaction distance, we may obtain a full analytical solution for the optimal free state entanglement levels, and for  $D_{\mathcal{F}}$  itself, for a four level system,  $\rho^{\text{int}}$ . A system of  $N$  single-particle entanglement levels,  $\{\epsilon_j\}$ , has a  $2^N \times 2^N$ -dimensional entanglement Hamiltonian,  $\hat{H}_E^f$ , with  $2^N$  levels in the many-body entanglement spectrum,  $\{E_j\}$ . Therefore, a free spectrum with four many-body levels has two single-particle levels,  $\epsilon_1$  and  $\epsilon_2$ , that build the full spectrum. It is convenient to work with probability densities,  $\rho^{\text{opt}} = e^{-\hat{H}_E^f}$ , allowing the single-particle energies to be defined as:  $b_1$  and  $b_2$ . The free many-body spectrum can then be built in the following way:

$$\begin{aligned} \rho_1^{\text{opt}} &= \left(\frac{1}{2} + b_1\right) \left(\frac{1}{2} + b_2\right), & \rho_2^{\text{opt}} &= \left(\frac{1}{2} - b_1\right) \left(\frac{1}{2} + b_2\right), \\ \rho_3^{\text{opt}} &= \left(\frac{1}{2} + b_1\right) \left(\frac{1}{2} - b_2\right), & \rho_4^{\text{opt}} &= \left(\frac{1}{2} - b_1\right) \left(\frac{1}{2} - b_2\right). \end{aligned}$$

To ensure the spectrum is normalised these levels are subject to  $\sum_j \rho_j^{\text{opt}} = 1$ , along with  $0 \leq b_1 \leq b_2 \leq \frac{1}{2}$  which fixes the ordering to that of interacting spectrum:  $0 \leq \rho_4^{\text{opt}} \leq \rho_3^{\text{opt}} \leq \rho_2^{\text{opt}} \leq \rho_1^{\text{opt}} \leq 1$ .

As a first attempt to minimise the interaction distance one may directly differentiate Eq. (1) of the main text, having substituted in the definitions above, to find the stationary points for some choice of parameters  $b_1$  and

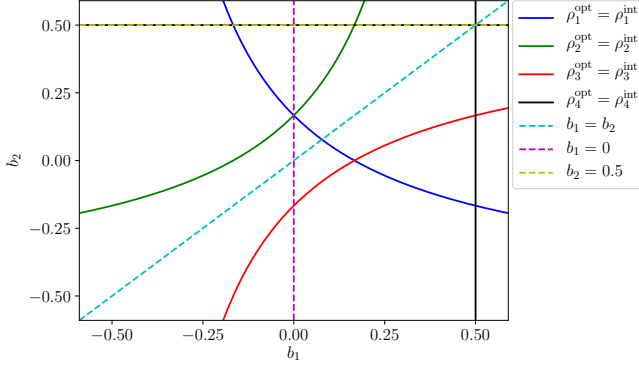


FIG. 6. Free parameter values,  $b_1, b_2$ , that produce boundary curves  $\rho_j^{\text{opt}} = \rho_j^{\text{int}}$  (solid lines) for  $\{\rho_j^{\text{int}}\} = \{\frac{1}{3}, \frac{1}{3}, \frac{1}{3}, 0\}$ . The dashed lines enclose the normalised and ordered regions for the free spectra. There are two points of intersection within the normalised and ordered region. The intersection that matches better the low level entanglement spectrum will give the most faithful representation of the interacting system. Thus, it is the  $b_1, b_2$  pair at the intersection between  $\rho_1^{\text{opt}} = \rho_1^{\text{int}}$  and  $\rho_2^{\text{opt}} = \rho_2^{\text{int}}$  that give the interaction distance,  $D_{\mathcal{F}} = \frac{1}{6}$ .

$b_2$ . These parameters contain all of the information required to build the free many body entanglement spectrum, so it is our goal to find the set that minimises  $D_{\mathcal{F}}$ . In doing so, we find that the derivatives are not defined in the regions  $\rho_j^{\text{opt}} = \rho_j^{\text{int}}$  for any  $j$ . We also find that second derivatives are always zero when  $\rho_j^{\text{opt}} \neq \rho_j^{\text{int}}$ , thus defining a saddle point and not a minimum. The minimum trace distance must therefore live on one of the boundary curves  $\rho_j^{\text{opt}} = \rho_j^{\text{int}}$  or an intersection of two or more curves. Of course, it is the low-level entanglement spectrum that provides important information about the system. Therefore, if it is possible to match the low levels then the optimal free state will more faithfully represent

the interacting system. In some cases, however, the intersection between the low level curves does not fall within the normalised and ordered region. In that case the most faithful representation lies on the curve  $b_1 = b_2$ .

An exhaustive analysis yields the following set of solutions for the interaction distance, where the superscript ‘int’ has now been dropped on all  $\rho_j^{\text{int}}$ :

$$D_{\mathcal{F}} = \begin{cases} 2\sqrt{\rho_1} - 2\rho_1 - \rho_2 - \rho_3, & \text{if } \rho_1 \geq (\rho_1 + \rho_2)^2 \\ \left| \frac{\rho_1\rho_4 - \rho_2\rho_3}{\rho_1 + \rho_2} \right|, & \text{otherwise.} \end{cases} \quad (\text{E1a})$$

and the following set of free parameter solutions:

$$(b_1, b_2) = \begin{cases} \left( \sqrt{\rho_1} - \frac{1}{2}, \sqrt{\rho_1} - \frac{1}{2} \right), & \text{if } \rho_1 \geq (\rho_1 + \rho_2)^2 \\ \left( \frac{\rho_1 - \rho_2}{2(\rho_1 + \rho_2)}, \rho_1 + \rho_2 - \frac{1}{2} \right), & \text{otherwise.} \end{cases} \quad (\text{E2a})$$

These exact solutions allow for an accurate study of the interaction distance without any error of numerical optimisation. The solutions (E1a) and (E1b) correspond to the cases where it is not possible and possible to match the lowest two levels of the entanglement spectrum, respectively.

In Fig. 6 we show an example of the boundary curves for the interacting spectrum  $\{\rho_j\} = \{\frac{1}{3}, \frac{1}{3}, \frac{1}{3}, 0\}$  that produces  $D_{\mathcal{F}} = \frac{1}{6}$ . We are able to deduce this solution by first considering the condition:  $\rho_1 \geq (\rho_1 + \rho_2)^2$ . For our set  $\{\rho_j\}$ , this inequality is not satisfied so  $b_1 \neq b_2$  and the minimum trace distance must therefore live at an intersection between the  $\rho_1^{\text{opt}} = \rho_1$  and  $\rho_2^{\text{opt}} = \rho_2$  curves. The pair  $b_1, b_2$  at this intersection result in the interaction distance.